Electronic Preprint for Journal of Information Processing Vol.30

Regular Paper

A Printable Soft-bodied Wriggle Robot with Frictional 2D-anisotropy Surface

Tung D. Ta[1,a)] Takuya Umedachi[2,b)] Michiyo Suzuki[3,c)] Yoshihiro Kawahara[1,d)]

Received: June 2, 2021, Accepted: December 3, 2021

Abstract: Soft-bodied animals move by using the anisotropic friction between their body and the environment. Inspired by these bodily structures, we propose a wriggle soft-bodied robot with an anisotropic frictional skin to support its locomotion. We combine soft and rigid materials in 3D printers to make different patterns of frictional anisotropy. We build a simulation model to predict the locomotion speed of the robot with different anisotropic frictional patterns. By using these patterns as the ventral side, we design a wriggle soft-bodied robot that can move 2.8 times faster than a robot with an omnidirectional frictional ventral surface. The fabrication time is less than one hour, and the locomotion speed is 0.17 body-lengths per second.

Keywords: frictional anisotropy, soft-bodied wriggle robots, body design and fabrication

1. Introduction

Designing contact friction is crucially essential in all soft-bodied animals and robots to realize desired functionalities such as locomotion and gripping. This is because soft-bodied animals and robots have larger contact areas with the environment and the operation target. This feature is in sharp contrast with the wheeled or traditional rigid robots, whose contact area is usually small spots on the rigid surface or the wheels. This difference is unavoidable in soft robots. Instead, the key to soft-bodied robot design is how to link the larger-surface interaction with the environments/objects to the desired functions. The success in pioneering soft robots previously proposed is due to the sophisticated design of the interaction between the larger contact area and the environments/objects inspired from the bodily structures of animals such as worms, octopus, fishes, elephants, and snakes [1], [17], [18], [22], [23].

The locomotion of soft-bodied robots is a very intriguing yet challenging theme. In this paper, to help explain contact friction design for soft robots, we will discuss the locomotion of string-like wheel-less soft-bodied robots inspired by worms and snakes. The agility of a snake makes it an object of a great deal of research into investigating and imitating its locomotion gaits [8], [10], [14], [19]. Although these research studies were inspired by the snake, these research efforts all focus on modeling the snake as a chain of multi-link rigid segments which results in a low degree of adaptability. Other research that modeled the snake body as a soft and deformable beam [25] showed a closer approximation to the locomotion of the real snake. However, that research assumed that the friction between the body of the snake and the ground is the same in every direction. To cover the behavior of the snake-like robot with non-uniform friction, some soft-bodied robots [15], [18] have passive wheels along their body to utilize the difference between rolling and sliding friction. Although this solution makes the undulation of the robots smoother, it also adds weight to the robot as well as lengthens the fabrication process.

The frictional anisotropy on the skin of worms and scales of snakes, as mentioned above, is suggested to effectively assist the locomotion. The animals can easily navigate on different surfaces by leveraging the anisotropic friction formed by the arrangement of the body axis [11]. One of the most straightforward ways to make an anisotropic frictional surface is to add a miniature tilted structure such as tilted hairs or nails surface [12], [16]. Nevertheless, these approaches are not strong and scalable enough to support the locomotion of a wriggle soft-bodied robot. In the case of tilted nails [12], the structure is strong but not printable. Furthermore, the tilted nails are more limited in the anisotropic frictional behavior. So it is difficult to scale up the structure to make an anisotropic frictional skin for the wriggling locomotion. In the case of tilted hairs in Ref. [16], the research is more focusing on the wetting property of the material at the microscopic scale. There is limited evidence that the tilted hairs structure of the nanofilm can support snake-like locomotion. Instead of adding tilted structures, the inching worm robot in Ref. [4] and the soft-bodied caterpillar-like robot [21] proposed printing combined soft-rigid materials structures that enable variable frictional legs to mimic the inching locomotion of a worm. However, in

1 Graduate School of Engineering, The University of Tokyo, Bunkyo, Tokyo 113–8656, Japan
2 Faculty of Textile Science and Technology, Shinshu University, Ueda, Nagano 386–8567, Japan
3 Department of Radiation-Applied Biology Research, Takasaki Advanced Radiation Research Institute, National Institutes for Quantum Science and Technology, Takasaki, Gunma 370–1292, Japan
a) tung@akg.t.u-tokyo.ac.jp
b) umedachi@shinshu-u.ac.jp
c) suzuki.michiyo@qst.go.jp
d) kawahara@akg.t.u-tokyo.ac.jp

these inching worm robots research efforts, the structures are only used for off-the-plane locomotion (i.e., inching) but not for in-the-plane locomotion such as serpentine locomotion.

In this research, we propose a 2D-anisotropic frictional structure that will support the undulation of a wriggling soft-bodied robot. In our approach, we take advantage of the multi-material 3D printing process to combine low-friction and high-friction material to realize the anisotropic frictional surfaces. The behavior of the anisotropic frictional surface can be easily tuned by changing the geometric parameters of the printed pattern. This design freedom allows us to design multiple anisotropic frictional surfaces to find the best one for wriggling locomotion. Our contributions include:

- A scheme to design 2D-anisotropic frictional surface to support serpentine locomotion,
- Fabrication and evaluation performance of a 2-segment wriggle soft-bodied robot with above frictional designed properties,
- Modeling and simulating the serpentine locomotion of a wriggling soft-bodied robot according to friction with the ground.

2. Soft-bodied Robot Design Using a 3D-printer

The robot body is a 3D-printed slender beam which is made of a rubber-like elastic material (as shown in **Fig. 1**). We design the ventral side of the robot with patterns of frictional anisotropy (as shown in **Fig. 2** and described in the following part). We use two DC motors, one in the front and one in the rear, to generate undulating movement of the body through four tendons which are attached to the fixture at the center of the body (as shown in **Fig. 3**).

2.1 2D-anisotropic Friction

Our 2D-anisotropic frictional surface comprises smaller circular 2D-anisotropic frictional elements with a radius r (as shown in Fig. 2 (a). The intervals between two neighboring circular elements are G. Each circular element, in turn, is divided into parts of different frictional material (high and low friction). We define α as the central angle of low friction circular sectors as shown in Fig. 2 (a) and Fig. 2 (b). From the side view, each circular element is extruded to become a rounded cylinder with height h. This design enables the ventral side of the robot to switch between high and low friction mode during the undulation (as shown in Fig. 2 (c), Fig. 2 (d), Fig. 2 (e)).

We use the Objet260 Connex3™ multi-material 3D printer

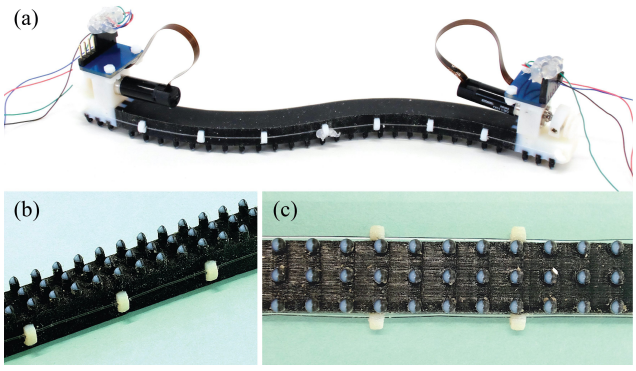

Fig. 1 Our soft-bodied wriggle robot is a 2-segment tendon-driven stringy robot that is fabricated from an elastic material. The robot uses a 2D-anisotropy frictional surface as its ventral to support the undulation locomotion. (a) The soft-bodied wriggle robot using the frictional 2D-anisotropy surface to support undulation locomotion. (b) Side-view of the 2D-anisotropic friction. (c) Combination of high/low materials to design the frictional 2D-anisotropy.

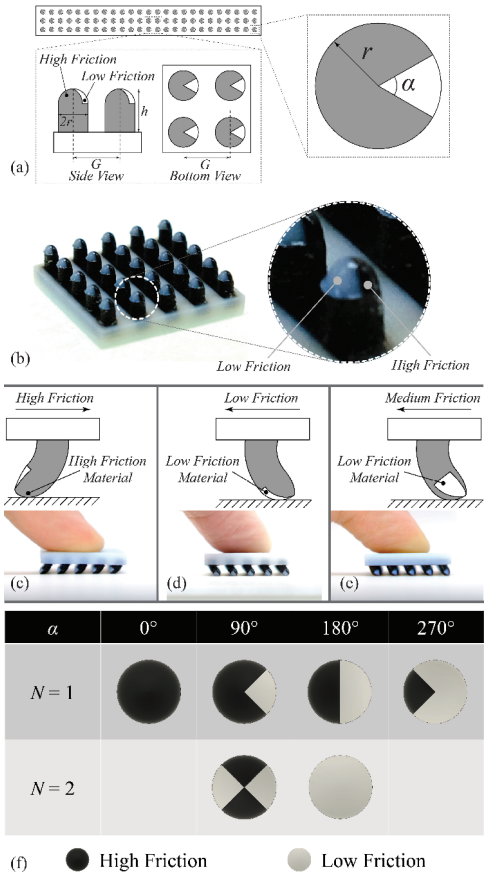

Fig. 2 The combination of the high and low friction material forms the 2D-anisotropic frictional surface. (a)–(b) The 2D-anisotropic friction surface consists of circular regions of radius r and spacing G. The shading part is high friction material, low friction material (white part) occupies a part of each region at angle α. From the side view, each circular region is a rounded-head cylinder of height h. (c)–(e) Bending of the rounded-head cylinder gives the entire surface anisotropic friction. (f) Different combinations of high (shading part) and low (white part) friction material controlled by the number N of α sectors of low friction material to form the 2D-anisotropic frictional surface.

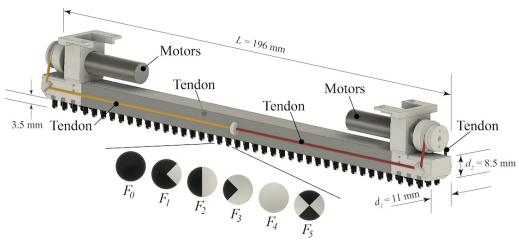

Fig. 3 The wriggle soft-bodied robot is a tendon-driven 196 mm × 11 mm × 8.5 mm elastic beam which is actuated by two motors at two ends of the beam. The ventral side of the robot is patterned with one of the six 2D-anisotropic frictional surfaces (F_0, F_1, F_2, F_3, F_4, F_5). The distribution and dimension (r = 1 mm, h = 3.5 mm, G = 5 mm) of the 2D-anisotropic frictional surfaces are described in Section 2.1.

with rigid polypropylene plastic-like material (VeroWhite™) as low friction material, and soft rubber-like material (TangoBlackPlus™) as high friction material [*1]. We also print the elastic body of the wriggle robot with TangoBlackPlus™. Figure 2 (b) shows a 3D printed sample of a square plate with 25 circular regions ($\alpha = 180°$, $r = 1$ mm, $h = 3.5$ mm, $G = 5$ mm). The frictional anisotropic behavior of this sample is shown in Fig. 2 (c), Fig. 2 (d), and Fig. 2 (e).

2.2 Parameters of The 2D-anisotropic Friction

Besides material factors such as friction coefficient and 3D printed material elasticity, we can design the frictional anisotropy of the surface described above and its influence on the locomotion of a wriggling robot by tuning the morphological parameters α, r, h, and G. However, for the simplicity of the analysis, we investigate only the effect from changing angle α whilst keeping all the other parameters fixed. In addition to parameter α, we introduce another parameter N which is the number of separated low frictional sectors in each circular element. In one circular element, we can add multiple separated sectors of low frictional material to achieve multi-directional anisotropic friction (as shown in Fig. 2 (f) in the case $N = 2$ and $\alpha = 90°$).

Although we can combine the two parameters α and N infinitely to design different 2D-anisotropic frictional surfaces, due to limitations on the 3D-printer resolution and the mechanical properties of the printing materials, we narrow down the list of combinations to $\alpha = \{0°, 90°, 180°, 270°\}$ and $N = \{1, 2\}$. Figure 2 (f) shows the configurations of all the combinations. We will find that these configurations are good enough to support the serpentine locomotion of a slender elastic wriggling soft-bodied robot.

3. Wriggling Robots Fabrication

3.1 Assembly

The main body of our wriggle soft-bodied robot is a 3D printed rubber-like (TangoBlackPlus™) slender beam with dimensions $L \times d_1 \times d_2 = 196\,\text{mm} \times 11\,\text{mm} \times 8.5\,\text{mm}$. The ventral side of the robot is patterned with 2D-anisotropic frictional surfaces as described above ($r = 1$ mm, $h = 3.5$ mm, $G = 5$ mm). Based on this design, we changed the values of parameter α and N to get robots with different locomotive behaviors (as shown in Fig. 3).

3.2 Undulation Generation

Our wriggle soft-bodied robot moves by undulating its body to mimic the serpentine locomotion of a snake. The undulation movement is generated by two bidirectional motors which are attached to two ends of the beam. Each motor will control two nylon tendons (diameter $\phi = 0.3$ mm) which run along the beam from the shaft of the motor to the center of the body as shown in Fig. 3. An Arduino controller board will control two motors to rotate clockwise/counterclockwise periodically, and thus, keep winding/unwinding the four tendons to bend the beam and generate periodical undulation as shown in **Fig. 4**.

In generating the undulation movement, we define:

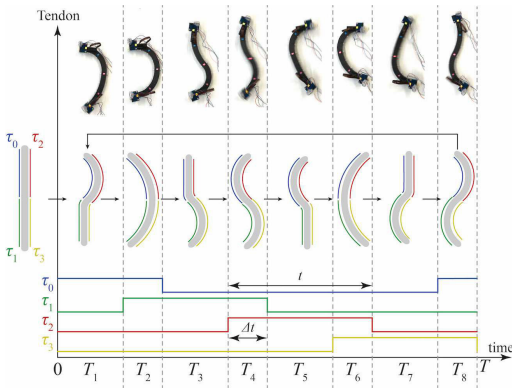

Fig. 4 By timely winding and unwinding two motors, we are able to sequentially bend parts of the beam to form an undulation movement. T is the period of the undulation, t is the time that a tendon is being wound, Δt is the time that two consecutive tendons are being wound.

- T: undulation period, the time of an undulation cycle,
- $T_i (i = 1, \ldots, 8)$: the time segment in one period corresponding to each of the 8 different actuation states of the four tendons (as shown in Fig. 4),
- t: on-time, the time that a tendon is being wound,
- Δt: overlapping-time, the time that two consecutive tendons are being wound, $-\infty \leq \Delta t \leq t$,
- ξ: the ratio $\Delta t/t$, $\xi \leq 1$.

Here, $\Delta t < 0$ means there is no overlapping on-time between two tendons and the time-span between the ending of on-state of a tendon and the beginning of on-state of the next tendon is $|\Delta t|$. Controlling t and Δt enables us to bend the beam into 8 different states as represented in each time slot in Fig. 4. From Fig. 4, it is shown that the wavelength of the traveling wave along the body is changing periodically (wavelength at T_2 is different with that at T_4) as we are using only two motors to control a 2-segment beam. A complete sinusoidal traveling wave can be generated using a 4-segment beam with 4 motors. However, we will show in the experiment that a 2-segment beam is enough to support the wriggling locomotion of the robots.

In this configuration, the ratio between overlapping-time and on-time ξ will affect the speed of the undulation.

- $\xi \leq 0$: there is no overlap in on-time of each pair of tendons. This leads to a discrete bending of the body which is not optimal for the locomotion speed of the robot.
- $0 < \xi \leq 0.5$: the higher ξ is, the faster the undulation wave travels. This means increasing ξ will increase the locomotion speed of the robot.
- $0.5 < \xi \leq 1$: this means there is an overlap between on-state of tendons τ_0 and τ_2, τ_1 and τ_3, which is not acceptable since one motor cannot rotate clockwise and counterclockwise at the same time.

Based on this analysis, we choose $\xi = 0.5$ to maximize the locomotion speed of the robot.

The two motors (Maxon 347726 DC Motor 8 mm 0.5 W) are controlled by an Arduino Nano board through a dual bidirectional motor driver chip (TB6612FNG, Toshiba) under an external 9 V DC power source. Each motor, when it is on, is set to rotate at maximum speed.

[*1] http://www.stratasys.com

4. Simulation

4.1 Simulation Model

We model the mechanical system of the wriggling robot (i.e., the deformable beam) as a mass-spring-damper system, in which eight mass points are linearly connected by a spring-damper and a torsion spring (**Fig. 5** (a)). All variables and parameters are listed in **Table 1**. The form factor parameters in the table were decided based on the prototype. Based on these values, we selected the other parameters (which are difficult to determine such as stiffness) by observing the movement of the simulator.

The bending motion is driven by altering the resting angle of variable torsion spring. To control the bending on the head side and the tail side independently, three variable torsion springs from the head (green) and three torsion springs from the back (red) shall be driven at different timings.

$$\begin{aligned}\Theta_{\text{head}} &= \pi + A\sin(\omega t)\\ \Theta_{\text{tail}} &= \pi + A\sin\left(\omega t - \frac{\pi}{2}\right)\end{aligned} \tag{1}$$

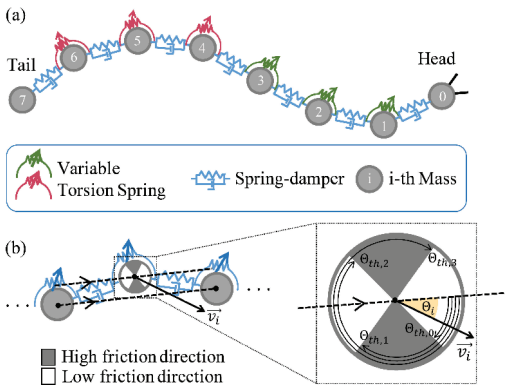

Fig. 5 (a) The mathematical model to simulate the locomotion of the robot, which is constructed with springs, masses, dampers, and torsion springs. (b) How the friction coefficient changes depending on the moving direction of particle i. The illustration exemplifies the F_5 pattern.

Table 1 Parameter used in Simulation.

Parameter	Description	Value
$m_{0,7}$	Mass of a anterior/posterior particle	12.0
m_i	Mass of the other particles	2.6
$c_{\text{gnd},i}$	Friction coefficient of particle i with the ground	Eq. (3)
c_{low}	Low friction coefficient	0.5
c_{high}	Low friction coefficient	2.5
ω	Intrinsic frequency of the resting angle variation	π
A	Amplitude coefficient of the resting angle variation	0.175π
$k_{\text{seg},i}$	Stiffness of the body axis springs	3.0×10^4
c_{seg}	Damping coefficient of the body axis springs	10.0
L_{seg}	Resting length of the body axis springs	22.5
$l_{\text{seg},i+\frac{1}{2}}$	Actual length of the body axis spring $i+\frac{1}{2}$	
k_{tor}	Stiffness of the torsion springs	1.0×10^5
$\Theta_{\text{tor},i}$	Resting angle of the torsion springs i	Eq. (1)
Θ_i	Actual angle of torsion spring i	

Position of the mass, $\vec{r}_i$ ($i = 0, \ldots, N-1$), is governed by the following equation:

$$\begin{aligned}m_i \frac{\mathrm{d}^2\vec{r}_i}{\mathrm{d}t^2} = &-\vec{F}_{\text{seg},i-\frac{1}{2}} + \vec{F}_{\text{seg},i+\frac{1}{2}}\\ &- \vec{F}_{\text{tor},i-1,i} + \vec{F}_{\text{tor},i,i} - \vec{F}_{\text{tor},i+1,i}\\ &- c_{\text{gnd},i}\cdot\vec{v}_i.\end{aligned} \tag{2}$$

$\vec{F}_{\text{seg},i+\frac{1}{2}}$ is force from body axis spring i. $\vec{F}_{\text{tor},n,i}$ is force on mass i from variable torsion spring n. $\vec{v}_i$ is the velocity of the mass i. $-c_{\text{gnd},i}\cdot\vec{v}_i$ is ground reaction force caused when the frictional 2D-anisotropy patterns contact with the ground, which is modeled by viscous friction. This modeling will be explained below.

We model the 2D-anisotropy surface with a switching friction coefficient depending on the moving direction, as illustrated in Fig. 5 (b) with the frictional patterns configuration parameters as shown in **Table 2**. The illustration is an example of F_5 pattern. Here, $\vec{v}_i = \frac{\mathrm{d}\vec{r}_i}{\mathrm{d}t}$. Considering the frictional 2D-anisotropy pattern is attached along the beam, we defined moving angle, Θ_i, based on

Table 2 2D-anisotropic frictional configuration parameters.

Pattern	$\Theta_{th,0}$	$\Theta_{th,1}$	$\Theta_{th,2}$	$\Theta_{th,3}$
F_0				
F_1	$\frac{\pi}{4}$	$\frac{7\pi}{4}$	2π	
F_2	$\frac{\pi}{2}$	$\frac{3\pi}{2}$	2π	
F_3	$\frac{3\pi}{4}$	$\frac{5\pi}{4}$	2π	
F_4	2π			
F_5	$\frac{\pi}{4}$	$\frac{3\pi}{4}$	$\frac{5\pi}{4}$	$\frac{7\pi}{4}$

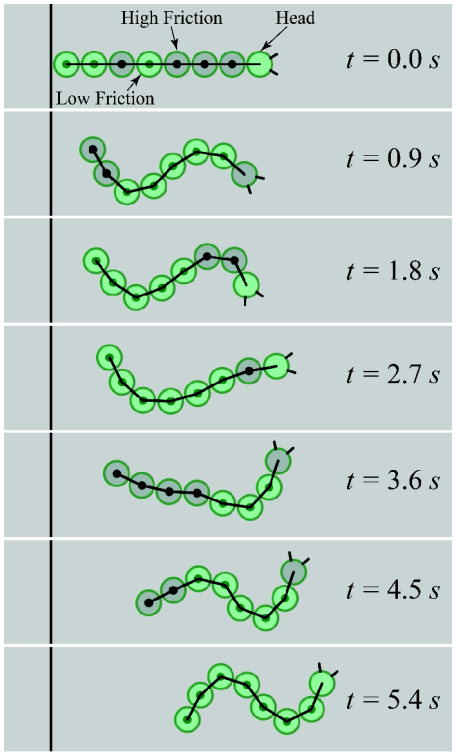

Fig. 6 A screenshot of the simulation running with pattern F_2. Green circles indicate particles which have low friction with the running surface. Shading circles indicate particles which have high friction with the running surface.

$\vec{v}_i$ and $\vec{r}_{i+1} - \vec{r}_{i-1}$. Frictional coefficient switches in conformance to the following equation:

$$c_{\mathrm{gnd},i} = \begin{cases} c_{\mathrm{low}} \text{ when } 0 \le \Theta_i \le \Theta_{th,0} \cup \Theta_{th,1} \le \Theta_i \le \Theta_{th,2} \\ \qquad \cup \Theta_{th,3} \le \Theta_i \le 2\pi \\ c_{\mathrm{high}} \text{ otherwise.} \end{cases} \quad (3)$$

4.2 Simulation Result

We set up the simulation with parameters and values as in Table 1. We let the simulator run for 20 seconds with each of the six different patterns of the 2D-anisotropic friction (from F_0 to F_5) and measure the traveled distance to calculate the average locomotion speed. **Figure 6** is a screenshot of the simulation running a robot model with the 2D-anisotropic frictional pattern F_2. The friction of each particle mass (shown as the green and shading color of the circles) depends on the frictional pattern, the curvature at each particle mass, and moving direction of each particle mass. The simulation speeds of all robot models are shown in **Fig. 9** with circular markers.

5. Experiment

To evaluate the performance of the 2D-anisotropic frictional design in supporting wriggling locomotion, we measure the locomotion speed of the wriggle soft-bodied robots with different patterns of the 2D-anisotropic frictional surface. The accompanying video shows footage of the locomotion of the wriggle soft-bodied robots.

5.1 Experiment Setup

5.1.1 2D-anisotropic Friction

We make six samples of the wriggling soft-bodied robots with six different 2D-anisotropic frictional patterns (from F_0 to F_5 as shown in Fig. 3) at the ventral surface. From this section onwards, we name the robots by their 2D-anisotropic frictional patterns as robot F_1, robot F_0. **Figure 7** shows a printed and actuating wriggling soft-bodied robot.

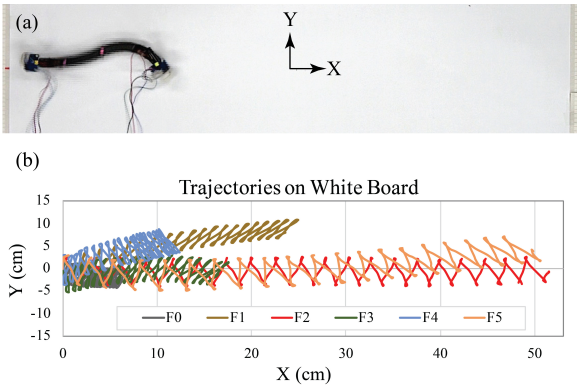

Fig. 7 (a) Each robot is put onto a horizontal flat rigid glassy surface. We run the robot for 20 s then measure its traveled distance. Each robot has markers so that we can analyze its locomotion using Kinovea. (b) Trajectory of the robots when running for 20 s on the experimental surface. On the XY plane of the experimental surfaces, each robot is placed along the X-axis so that one end of the robot is positioned at point $(0, 0)$. The robots are controlled to move in the same direction as the positive X-axis.

5.1.2 Controlling Parameter

Through the preliminary test, we found that due to the mechanical properties of the printing material and the morphology of the body of the robot, it takes about 0.5 seconds for one segment of the robot to bend from the resting state to the maximum bent state. Therefore, we set the on-time $t = 500$ ms. The specific values of the controlling parameters are listed in **Table 3**.

5.1.3 Experiment Environment

We tested the locomotion of our robot on a rigid glossy whiteboard surface. The friction coefficients between each ventral pattern with the surface are listed in **Fig. 8**. We calculate the average locomotion speed of the robot based on the distance it traveled in 20 seconds. Each test is recorded by a camera (Sony Handycam FDR-AX55 [*2]). We add markers to the robot as Fig. 7 (a) and analyze the trajectories as well as the speed of the robots using OpenCV [*3].

5.2 Experiment Result

We are able to generate stable undulating movement for all six types of robots. Figure 4 is a graph showing the locomotion of robot F_1.

5.2.1 Locomotion Speed

Figure 7 (b) shows the trajectory of each robot when running for 20 seconds on the experimental surface. Although all of the robots manage to move forward, the locomotion speed and trajectories vary.

Robot F_2 has the most stable direction of locomotion (as shown in Fig. 7 (b)) while others are veering away from the designated horizontal route. We believe that the reason for the stable locomotion direction is that the difference between directional friction coefficients (μ_f, μ_b, μ_t) in case of F_2 is larger than that of the others. Although these differences in robot F_1 are also large, the speed and stability of the direction of the locomotion worsen due to the high transverse friction coefficient μ_t which makes it more difficult to bend. As evidently shown in Fig. 9, the locomotion

Table 3 Setup values of controlling parameters.

Parameter	Value
Tendon on-time t	500 ms
Tendon overlapping-time Δt	$0.5t = 250$ ms
Motor speed	Maximum (PWM = 255)
Tendon length at rest	75 mm

	μ_f	μ_b	μ_t
F0	2.25	2.25	2.25
F1	0.70	1.28	1.28
F2	0.90	1.88	1.39
F3	0.42	0.58	0.42
F4	0.42	0.42	0.42
F5	0.70	0.70	0.75

Fig. 8 The friction coefficient of ventral pattern on the experimental surfaces in forward direction μ_f, backward direction μ_b, and transverse direction μ_t. Reddish cells indicate a high friction coefficient. Greenish cells indicate a low friction coefficient.

[*2] http://sony.jp
[*3] https://opencv.org/

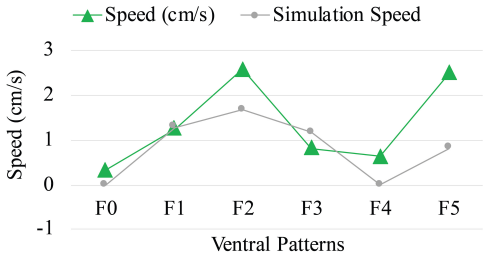

Fig. 9 The locomotion speeds of the robots (different 2D-anisotropic frictional surfaces) during the experiment and simulation are closely matched.

speed of the robot and the simulation closely match each other. In both of the cases, the robot F_2 has the highest average locomotion speed. In the experiment with the real robot, the robot F_2 is eight times faster than the slowest design F_0. Undulation has little effect in the case of F_0 since its ventral is printed completely with high friction material. Another good performer is the robot F_5. Although the trajectory of robot F_5 is not as stable as that of robot F_2, the locomotion speeds are in the same order. This suggests that the transverse high friction might make a larger contribution than backward high friction to the locomotion speed of the robot.

A deeper quantitative analysis is necessary to explain the reason behind the difference in the performance of each pattern. Here, we will try to give a qualitative explanation for the performance of the robots F_2 and F_5. Both patterns help the robot slide easier forward, but more difficult to slide laterally. We believe that depending on the bending angle of the body of the robot, there is an optimal profile for the low-friction/high-friction materials. In our setup, that optimal profile is manifested in pattern F_2. In the case of F_5, it is interesting that F_5 outperforms F_1 even though these seem to be similar. This difference can be partially explained as a result of the dominance of high-friction material in F_1. A large high-frictional region such as that in F_1 makes the undulation trajectory unstable and in general, reduces the average locomotion speed.

6. Discussion

We have proposed a robot with specifically designed 2D-anisotropic surfaces which significantly affect the locomotion speed of the robot. The result of the experiment, as shown in Fig. 9, indicates that, in many animals and robots, having a rational structure of friction, such as scales and tilted hair, is crucial to move efficiently. Our wriggle robot can be used in studying locomotion of small and stringy undulators which, otherwise, are difficult to analyze. One example is the locomotion of the nematode *Caenorhabditis elegans*. The outer surface of *C. elegans* [3] is covered by a tough but flexible extracellular cuticle. This cuticle protects the animal from the surrounding environment, maintains its body shape, and enables motility by acting as an external skeleton. The cuticle surface bears shallow, circumferentially-oriented furrows [7] and its structure can only be observed using a scanning electron microscope (SEM), transmission electron microscope (TEM), or atomic force microscope (AFM) images. Hundreds of these furrows (which cause unevenness) are oriented "perpendicularly" to the midline, and that allows the worm to grip water on the surface of the floor (agar). The fact that these stripes

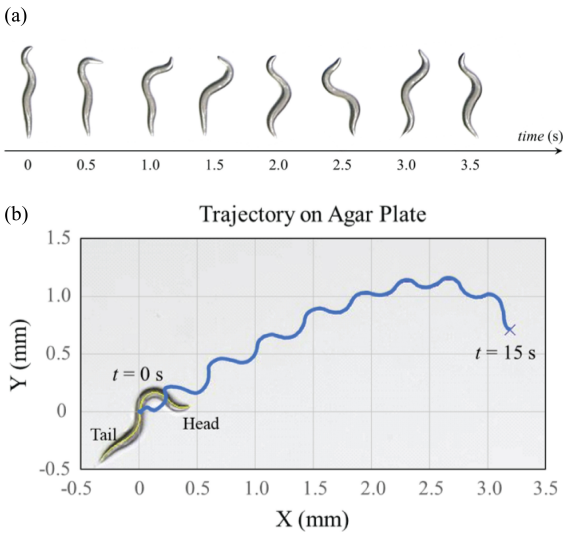

Fig. 10 (a) Body form of an adult *C. elegans* in forward motion on an agar plate—nematode growth medium—as acquired every 0.5 s for a 3.5 s period. (b) Trajectory of the mid-point of the body of an adult *C. elegans* over a 15 s period of locomotion.

are engraved regularly at an extremely thin pitch perpendicular to the midline may increase the efficiency of movement when using friction. Measuring the frictional anisotropy of creatures this size is a difficult task and almost impossible. The pattern seems to be a structure that makes it hard to slip along the body axis and easy to slip in the direction perpendicular to the body axis. Is this conjecture true?

The body form of an adult *C. elegans* in forward locomotion on an agar plate [3] as measured every 0.5 s for 3.5 s is shown in **Fig. 10** (a). Furthermore, the trajectory of the mid-point of the body of this worm over a 15 s period is plotted in Fig. 10 (b). When compared with the trajectories of a soft-bodied wriggle robot, it appears that the worm traces a sinusoidal wave pattern and moves more smoothly on the agar surface using friction. This smooth movement may be related to the fact that the area touching the surface of the floor (agar) is wider than that in the case of a soft-bodied wriggle robot.

In the experiments using our proposed soft-bodied wriggle robot, patterns F_2 and F_5 allowed the robot to move speedily in a manner similar to the *C. elegans*. These results indicate that the surface pattern of *C. elegans*, contrary to the above-mentioned expectations, realizes the same frictional anisotropy as F_2 or F_5. Animals and robots using these scales and hairs often display the frictional patterns such as F_2 and F_5. There is a possibility that *C. elegans* may also have these common properties, even though visual observation of the body structure suggests differently.

By proposing the wriggle robot, we present the possibility that we can determine some common rules of locomotion through comparison of the movements of a robot with those of actual worms. In *C. elegans*, backward locomotion is known to be somewhat faster than forwarding locomotion. The research of the locomotion of gastropods [13] proposed methods to measure the traction force of small creatures crawling on a flat surface. However, due to the difference in the scale of the gastropods and *C. elegans*, it is still challenging to measure the friction between the body of the worm and the floor. More improvement in the

Table 4 Comparison to other wriggle robots.

Robot	Max Speed (mm/s)	Weight (kg)	Length (mm)	Rigid or Soft	Frequency (Hz)
ACM R1 [6]	1,000	28	2,430	Rigid	> 0.25
AmphiBot II [5]	400		772	Rigid	1.00
Koryu II [9]	500	350	3,300	Rigid	NA
OmniTread OT-8 [2]	100	13.6	1,270	Rigid	NA
Onal's FEA Snake Robot [18]	19		280	Soft	0.25
Our wriggle Robot	26	0.238	196	Soft	1.00

measurement setup will be needed to measure the traction force of the crawling worm. Currently, there is insufficient evidence to explain the relationship between the surface shape of the worm and the ease of its backward locomotion. By addressing this problem using our proposed soft robot, in which surface friction can be freely designed, and/or the estimation method with a mathematical model [20] rather than using the actual measurements, it may be possible to investigate how friction contributes to the movements of worm in the future.

7. Future Works

The frictional 2D-anisotropic surface helps support the locomotion of a wriggle soft-bodied robot. Among existing wriggle rigid/soft robots, our wriggle soft-bodied robot fits in the class of the small size crawling robot as shown in **Table 4**. In total, our robot's weight is 238 grams and has the length of 196 mm. By designing the whole body as a continuum beam, we can take advantage of 3D printing technology to shrink down the fabrication time of the robot. The fact that our robot is soft makes it more promising in adapting to different environments, especially spatial limited spaces. Our robots need to wriggle with a higher frequency than other wriggling robots. This is understandable since our robots use printed anisotropic frictional surfaces rather than bulky passive wheels that are used in other wriggling robots.

In the future, we will improve the robots as follows:

- Miniaturization: the frictional force between the robot and the ground depends on the weight of the robot as well as the contacting area. Exploring the effects of the frictional 2D-anisotropic surface in miniaturized crawling soft-bodied robots will give a better insight into how to design with the frictional anisotropy.
- Beam elasticity: elasticity of the beam has a large impact on the curvature of the undulation as well as the speed of the traveling wave. This raises the question about how can we design and control the undulation to get the optimal performance of the soft-bodied wriggle robot.
- Backward locomotion: Backward locomotion is not a common locomotive behavior in snakes but can be found in other creatures that travel by lateral undulation (such as *C. elegans* [24]). In our experiment, we note that though robot F_5 although does not have the highest locomotion speed, it does have this backward locomotion mode thanks to its symmetry along a directional friction surface. F_5 has bi-directionally low friction along the beam and high friction transversely. Therefore, just by switching the direction of the undulation wave propagation, we can make F_5 moving forward or backward.
- Other parameters: in this research, we deliberately fix all parameters except α and N. A thorough investigation of how other factors affect the locomotion of the wriggle soft-bodied robot is necessary to design a highly adaptive robot. These additional patterns are also useful in the investigation of *C. elegans* locomotion behaviors through our robotic models.

8. Conclusions

In this paper, we propose a scheme for designing and fabricating a group of different 2D-anisotropic frictional patterns which will support the serpentine locomotion of a 2-segment wriggling soft-bodied robot. We also build a simulation to analyze the influence of the 2D-anisotropic friction on the speed and the direction of the locomotion. We found that the experiment with a real robot closely matches up with the simulation. In both cases, we found that the design of half low frictional material and half high frictional material (robot F_2) will give the fastest and most stable locomotion. Our 2D-anisotropic friction and the robot itself can be printed with a 3D printer in less than one hour.

Acknowledgments This work was supported by JST ERATO Grant Number JPMJER1501, Japan, Science of Softrobotics (18H05467), Japan and JSPS Grant-in-Aid for Scientific Research on Innovative Areas, The Ministry of Education, Culture, Sports, Science and Technology (MEXT), and JSPS Grant-in-Aid for Young Researcher Grant Number 20K14690, Japan. The authors thank the Caenorhabditis Genetic Center for providing a wild-type N2 strain of *C. elegans*.

References

[1] Bayani, S., Rastegari, R. and Samavati, F.C.: Design of hyper redundant robot using ball screw mechanism approach, *2015 IEEE International Conference on Advanced Intelligent Mechatronics* (*AIM*), pp.1271–1276 (online), DOI: 10.1109/AIM.2015.7222713 (2015).

[2] Borenstein, J., Granosik, G. and Hansen, M.: The OmniTread serpentine robot: Design and field performance, *Unmanned Ground Vehicle Technology VII*, Gerhart, G.R., Shoemaker, C.M. and Gage, D.W. (Eds.), SPIE (2005).

[3] Brenner, S.: The genetics of Caenorhabditis elegans, *Genetics*, Vol.77, No.1, pp.71–94 (1974).

[4] Cheng, N., Ishigami, G., Hawthorne, S., Chen, H., Hansen, M., Telleria, M., Playter, R. and Iagnemma, K.: Design and analysis of a soft mobile robot composed of multiple thermally activated joints driven by a single actuator, *2010 IEEE International Conference on Robotics and Automation*, pp.5207–5212 (2010).

[5] Crespi, A. and Ijspeert, A.J.: AmphiBot II: An amphibious snake robot that crawls and swims using a central pattern generator, *Proc. 9th International Conference on Climbing and Walking Robots* (*CLAWAR* 2006), pp.19–27 (2006).

[6] Endo, G., Togawa, K. and Hirose, S.: Study on self-contained and

terrain adaptive active cord mechanism, *Proc. 1999 IEEE/RSJ International Conference on Intelligent Robots and Systems, Human and Environment Friendly Robots with High Intelligence and Emotional Quotients* (*Cat. No.99CH36289*), Vol.3, pp.1399–1405 (1999).
[7] Hall, D.H. and Altun, Z.F.: *C. elegans Atlas*, Cold Spring Harbor Laboratory Press (2008).
[8] Hirose, S. and Mori, M.: Biologically Inspired Snake-like Robots, *2004 IEEE International Conference on Robotics and Biomimetics*, pp.1–7 (online), DOI: 10.1109/ROBIO.2004.1521742 (2004).
[9] Hirose, S., Morishima, A., Tukagosi, S., Tsumaki, T. and Monobe, H.: Design of practical snake vehicle: Articulated body mobile robot KR-II, *Fifth International Conference on Advanced Robotics 'Robots in Unstructured Environments*, Vol.1, pp.833–838 (1991).
[10] Hirose, S.: *Biologically Inspired Robots: Snake-Like Locomotors and Manipulators*, Oxford Univ. Press (online), DOI: 10.1017/S0263574700017264 (1993).
[11] Hu, D.L., Nirody, J., Scott, T. and Shelley, M.J.: The mechanics of slithering locomotion, *Proc. National Academy of Sciences*, Vol.106, No.25, pp.10081–10085 (online), DOI: 10.1073/pnas.0812533106 (2009).
[12] Khan, R., Watanabe, M. and Shafie, A.A.: Kinematics Model of Snake Robot Considering Snake Scale, *American Journal of Applied Sciences*, Vol.7, No.5, pp.669–674 (online), DOI: 10.3844/ajassp.2010.669.674 (2010).
[13] Lai, J.H., del Alamo, J.C., Rodríguez-Rodríguez, J. and Lasheras, J.C.: The mechanics of the adhesive locomotion of terrestrial gastropods, *J. Exp. Biol.*, Vol.213, No.Pt 22, pp.3920–3933 (2010).
[14] Liu, C.Y. and Liao, W.H.: A Snake Robot Using Shape Memory Alloys, *2004 IEEE International Conference on Robotics and Biomimetics*, pp.601–605 (online), DOI: 10.1109/ROBIO.2004.1521848 (2004).
[15] Luo, M., Pan, Y., Skorina, E.H., Tao, W., Chen, F., Ozel, S. and Onal, C.D.: Slithering towards autonomy: A self-contained soft robotic snake platform with integrated curvature sensing, *Bioinspiration & Biomimetics*, Vol.10, No.5, p.055001 (2015) (online), available from ⟨http://stacks.iop.org/1748-3190/10/i=5/a=055001⟩.
[16] Malvadkar, N.A., Hancock, M.J., Sekeroglu, K., Dressick, W.J. and Demirel, M.C.: An engineered anisotropic nanofilm with unidirectional wetting properties, *Nature Materials*, Vol.9, pp.1023–1028 (online), DOI: 10.1038/nmat2864 (2010).
[17] Marchese, A.D., Onal, C.D. and Rus, D.: Autonomous Soft Robotic Fish Capable of Escape Maneuvers Using Fluidic Elastomer Actuators, *Soft Robot*, Vol.1, No.1, pp.75–87 (online), DOI: 10.1089/soro.2013.0009 (2014).
[18] Onal, C.D. and Rus, D.: Autonomous undulatory serpentine locomotion utilizing body dynamics of a fluidic soft robot, *Bioinspiration & Biomimetics*, Vol.8, No.2, p.026003 (online), DOI: 10.1088/1748-3182/8/2/026003 (2013).
[19] Sato, M., Fukaya, M. and Iwasaki, T.: Serpentine locomotion with robotic snakes, *IEEE Control Systems*, Vol.22, No.1, pp.64–81 (online), DOI: 10.1109/37.980248 (2002).
[20] Soh, Z., Suzuki, M. and Tsuji, T.: An Estimation Method for Environmental Friction Based on Body Dynamic Model of Caenorhabditis elegans, *Journal of Robotics, Networking and Artificial Life*, Vol.4, No.1, pp.32–40 (2017).
[21] Umedachi, T. and Trimmer, B.A.: Design of a 3D-printed soft robot with posture and steering control, *2014 IEEE International Conference on Robotics and Automation* (*ICRA*), pp.2874–2879 (online), DOI: 10.1109/ICRA.2014.6907272 (2014).
[22] Umedachi, T., Vikas, V. and Trimmer, B.A.: Highly deformable 3-D printed soft robot generating inching and crawling locomotions with variable friction legs, *2013 IEEE/RSJ International Conference on Intelligent Robots and Systems*, pp.4590–4595 (online), DOI: 10.1109/IROS.2013.6697016 (2013).
[23] Wehner, M., Truby, R.L., Fitzgerald, D.J., Mosadegh, B., Whitesides, G.M., Lewis, J.A. and Wood, R.J.: An integrated design and fabrication strategy for entirely soft, autonomous robots, *Nature*, Vol.536, No.7617, pp.451–455 (online), DOI: 10.1038/nature19100 (2016).
[24] Zhen, M. and Samuel, A.D.: *C. elegans* locomotion: Small circuits, complex functions, *Current Opinion in Neurobiology*, Vol.33, pp.117–126 (online), DOI: 10.1016/j.conb.2015.03.009 (2015).
[25] Zhu, L., Cao, Y., Liu, Y., Yang, Z. and Chen, X.: Architectures of soft robotic locomotion enabled by simple mechanical principles, *Soft Matter*, Vol.13, pp.4441–4456 (online), DOI: 10.1039/C7SM00636E (2017).

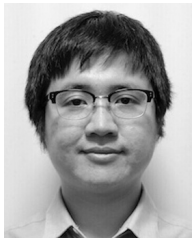

Tung D. Ta is a researcher in the Department of Electrical Engineering and Information Systems, Graduate School of Engineering, The University of Tokyo. His research interests are in the fields of digital fabrication, flexible electronic circuits and soft-bodied robotics. He received his Ph.D. in Information Communication Engineering – The University of Tokyo in 2019, M.E. in 2016, and B.E. from the department of Software Engineering – FPT University in 2012. He is a member of ACM, IEEE, IPSJ, and IEICE.

Takuya Umedachi is a soft-roboticist inspired by primitive living organisms such as amoeba and caterpillars. His research focus on decentralized control and self-formation of soft-bodied animals, which are modeled and verified by developing robotic testbeds with digital fabrication (including 3D printing and Printed electronics). He received a Ph.D. degree in Electrical and Communication Engineering from Tohoku University, in 2009.

Michiyo Suzuki is a principal researcher in the Department of Radiation-Applied Biology Research, Takasaki Advanced Radiation Research Institute, National Institutes for Quantum Science and Technology (QST). Her research interests are in the studying of the neural system of the nematode *Caenorhabditis elegans* using radiation. She focuses on development of the mathematic models for simulating the neural circuit of the *C. elegans*. She received her Ph.D. in Systems Engineering in 2006, M.A. in 2003, and B.Ed. in 2001, respectively. She is a member of IEEE.

Yoshihiro Kawahara is a Professor in the Department of Electrical Engineering and Information Systems, Graduate School of Engineering The University of Tokyo. His research interests are in the areas of Computer Networks and Ubiquitous and Mobile Computing. He is currently interested in developing energetically autonomous information communication devices. Even though wireless communication technology advances, the terminals are still tethered by power cords. He is trying to eliminate the power cords by the Energy Harvesting and the Wireless Power Transmission. He received his Ph.D. in Information Communication Engineering in 2005, M.E. in 2002, and B.E. in 2000. He joined the faculty in 2005. He is a member of IEICE, IPSJ, ACM, and IEEE. He is a committee member of IEEE MTT TC-24 (RFID Technologies).